ResearchGate

See discussions, stats, and author profiles for this publication at: https://www.researchgate.net/publication/320386986

The permittivity and refractive index measurements of doped barium titanate (BT-BCN)

Article *in* Optical Materials · November 2017

DOI: 10.1016/j.optmat.2017.09.040

CITATIONS
0

READS
35

11 authors, including:

Deepam Maurya
Virginia Polytechnic Institute and State Unive…
104 PUBLICATIONS **958** CITATIONS

SEE PROFILE

Min-Gyu Kang
Virginia Polytechnic Institute and State Univ…
56 PUBLICATIONS **309** CITATIONS

SEE PROFILE

Michael Clavel
Virginia Polytechnic Institute and State Unive…
25 PUBLICATIONS **102** CITATIONS

SEE PROFILE

Some of the authors of this publication are also working on these related projects:

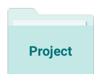

Piezoelectric Sensors and Energy Harvesters for Internet of Things (IoT) View project

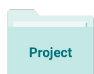

Darpa Matrix View project

All content following this page was uploaded by Deepam Maurya on 13 October 2017.

The user has requested enhancement of the downloaded file.

Optical Materials 73 (2017) 793–798

Contents lists available at ScienceDirect

Optical Materials

journal homepage: www.elsevier.com/locate/optmat

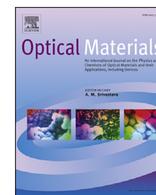

The permittivity and refractive index measurements of doped barium titanate (BT-BCN)

Michael A. Meeker [a], Souvik Kundu [b, 1], Deepam Maurya [b], Min-Gyu Kang [b], Alejandro Sosa [a], Rathsara R.H.H. Mudiyanselage [a], Michael Clavel [c], Sreenivasulu Gollapudi [b], Mantu K. Hudait [c], Shashank Priya [b], Giti A. Khodaparast [a, *]

[a] Department of Physics, Virginia Tech, Blacksburg, VA, 24061, USA
[b] Center for Energy Harvesting Materials and Systems (CEHMS), Department of Mechanical Engineering, Virginia Tech, Blacksburg, VA, 24061, USA
[c] Advanced Devices & Sustainable Energy Laboratory (ADSEL), Bradley Department of Electrical and Computer Engineering, Virginia Tech, Blacksburg, VA, 24061, USA

A R T I C L E I N F O

Article history:
Received 3 July 2017
Received in revised form
19 September 2017
Accepted 22 September 2017

Keywords:
Barium titanate
Ferroelectrics
Random access memory

A B S T R A C T

While piezoelectric- ferroelectric materials offer great potential for nonvolatile random access memory, most commonly implemented ferroelectrics contain lead which imposes a challenge in meeting environmental regulations. One promising candidate for lead-free, ferroelectric material based memory is $(1-x)BaTiO_3 - xBa(Cu_{1/3}Nb_{2/3})O_3$ (BT-BCN), $x = 0.025$. The samples studied here were grown on a Si substrate with an HfO_2 buffer layer, thereby preventing the interdiffusion of BT-BTCN into Si. This study provides further insight into the physical behavior of BT-BCN that will strengthen the foundation for developing switching devices. The sample thicknesses ranged from 1.5 to 120 nm, and piezoelectric force microscopy was employed in order to understand the local ferroelectric behaviors. Dielectric constant as a function of frequency demonstrated enhanced frequency dispersion indicating the polar nature of the composition. The relative permittivity was found to change significantly with varying bias voltage and exhibited a tunability of 82%. The difference in the peak position during up and down sweeps is due to the presence of the spontaneous polarization. Furthermore, reflectometry was performed to determine the refractive index of samples with differing thicknesses. Our results demonstrate that refractive indices are similar to that of barium titanate. This is a promising result indicating that improved ferroelectric properties are obtained without compromising the optical properties.

© 2017 Elsevier B.V. All rights reserved.

1. Introduction

Ferroelectric (FE) materials are promising candidates for random access memory devices due to their non-volatile properties, allowing for significantly higher data retention times compared to dynamic access memory [1–6]. They also offer significantly faster possessing times and higher endurance compared to flash [1,2,7]. However, two main concerns facing the implementation of FE random access memory (FeRAM) are the limited availability of lead-free FE materials and the possibility of a destructive readout process [2]. One possible material candidate for FeRAM applications is the lead-free compound $BaTiO_3$ (BTO). We have shown that when BTO is doped with $Ba(Cu_{1/3}Nb_{2/3})O_3$ to form $(1-x)BaTiO_3 - xBa(Cu_{1/3}Nb_{2/3})O_3$ (BT-BCN), $x = 0.025$, its piezoelectric response is enhanced [8–10]. The local crystallographic distortions in bulk BT-BCN were found to play a major role in giving rise to enhanced piezoelectric response, as observed through the change in the local lattice dynamics and hyperfine splitting [8]. The overall enhanced piezoelectric response in the bulk system was attributed to the synergic effects of the polar distortions, distribution of polar nano-regions, and domain confinement.

Furthermore, to maintain charge neutrality in BT-BCN, the formation of the defect dipoles was reported [8–10], which were aligned along crystallographic c-axis and found to play important role in governing the field-dependent response. We expect these defect dipoles, along with other charged defects, resulted in

* Corresponding author.
E-mail address: khoda@vt.edu (G.A. Khodaparast).
[1] Current address: Department of Electrical Electronics Engineering, BITS-Pilani (Hyderabad Campus), Telangana, 500078, India.

https://doi.org/10.1016/j.optmat.2017.09.040
0925-3467/© 2017 Elsevier B.V. All rights reserved.

internal bias and modulated electrical transport behavior. These defect dipoles can modulate the optical response of the system, and thus this study focuses on quantifying the variation in the dielectric permittivity and the optical response.

In our prior study, the ferroelectric properties of BT-BCN thin films were measured and its potential applications in nonvolatile memory devices was elucidated [11]. Apart from this electronic memory application, current research interest also lies in the fabrication of lead-free ferroelectrics, and in implementation of nondestructive readout utilizing electro-optical (EO) properties of FE materials [12,13]. In the literature, there is no report available on determining EO coefficients of BT-BCN thin films, though BT-BCN offers several advantages over BTO [8,9,11,14]. In this study, first we demonstrate the integration of the ferroelectric BT-BCN thin films on Si, with an HfO_2 buffer layer. Next, FE behavior was characterized using domain switching through piezoelectric force microscopy (PFM) measurements and dielectric permittivity, and lastly, reflectometry measurements were performed in order to measure the index of refraction. This study sheds light towards developing opto-integrated circuits on Si using a lead free FE.

2. Samples

Atomic layer deposition was used to grow 10 nm thick HfO_2 layers at 250 °C on a p-Si substrate, while BT-BCN was deposited by pulsed laser deposition (PLD) at temperatures ranging from 750 to 800 °C. The BT-BCN target (for PLD) was synthesized using the conventional solid state reaction method [11]. In order to investigate microstructure, cross-sectional scanning electron micrographs (SEM) were recorded using a LEO Zeiss 1550 (Zeiss, Munich, Germany) microscope. To avoid charging during microscopy, a palladium-gold coating was applied on the film surface. Fig. 1a) and b) show SEM cross-sectional micrographs of the two BT-BCN films with thicknesses of 120 and 90 nm, respectively. Fig. 1c shows transmission electron microscopic image of the sample exhibiting HfO_2 buffer layer and columnar growth of the films. Fig. 1d shows the elemental analysis of the film where one can clearly see clean interface of the film, buffer layer (HfO_2) and the substrate. Furthermore, the BT-BCN film with higher thickness could have reduced clamping from the substrate and may exhibit superior functional response and relative permittivity. The enhanced piezoelectric response is accompanied with enhanced relative permittivity, which in turn is related to the refractive index of the system.

3. Experimental details

3.1. Piezoelectric force microscopy

In order to quantify the local ferroelectricity in BT-BCN, we employed PFM (SCM-PIT, Bruker) to probe the local domain configurations and understand the polarization switching behavior. The PFM topography obtained from the surface of BT-BCN thin film is shown in Fig. 2. Fig. 2a) shows the amplitude micrograph of the 90 nm thick film, and Fig. 2d) displays the amplitude as a function of tip bias. Fig. 2b) and c) show the PFM phase micrographs, with the polarization of the central region in Fig. 2c) being reversed compared to Fig. 2b). In these micrographs, polarization is downward in the dark region and is upward where the region is yellow, affirming the 180° phase difference between two domains [11,15]. The out-of-plane piezoresponse was recorded as a function of applied voltage. The PFM hysteresis loop in amplitude is shown in Fig. 2d), whereas, Fig. 2e) depicts the hysteresis loop in phase. These results establish the ferroelectricity in BT-BCN thin films. In prior work, we have also demonstrated the polarization inversion in BT-BCN ceramics [11]. It is noteworthy to mention that domain

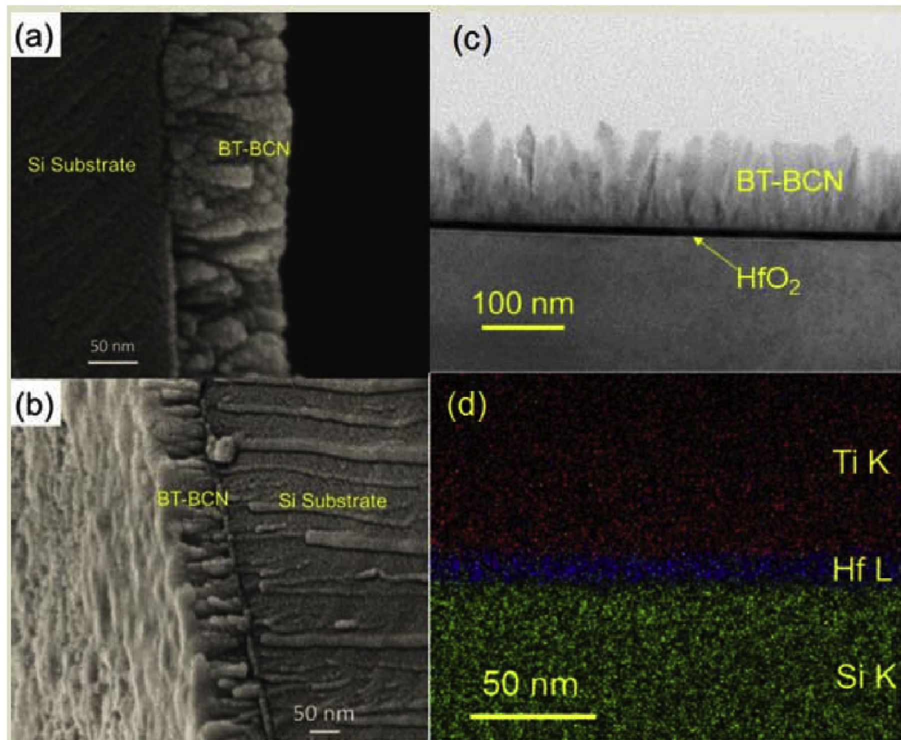

Fig. 1. SEM measurements for two samples, with growth temperatures of 800 °C and 750 °C for panel a) and panel b), respectively. The thickness of the layer in sample a) is 120 nm, while the thickness of the film in b) is 90 nm c) Bright field TEM image. d) Elemental mapping across the interface, indicating diffusion free interfaces.

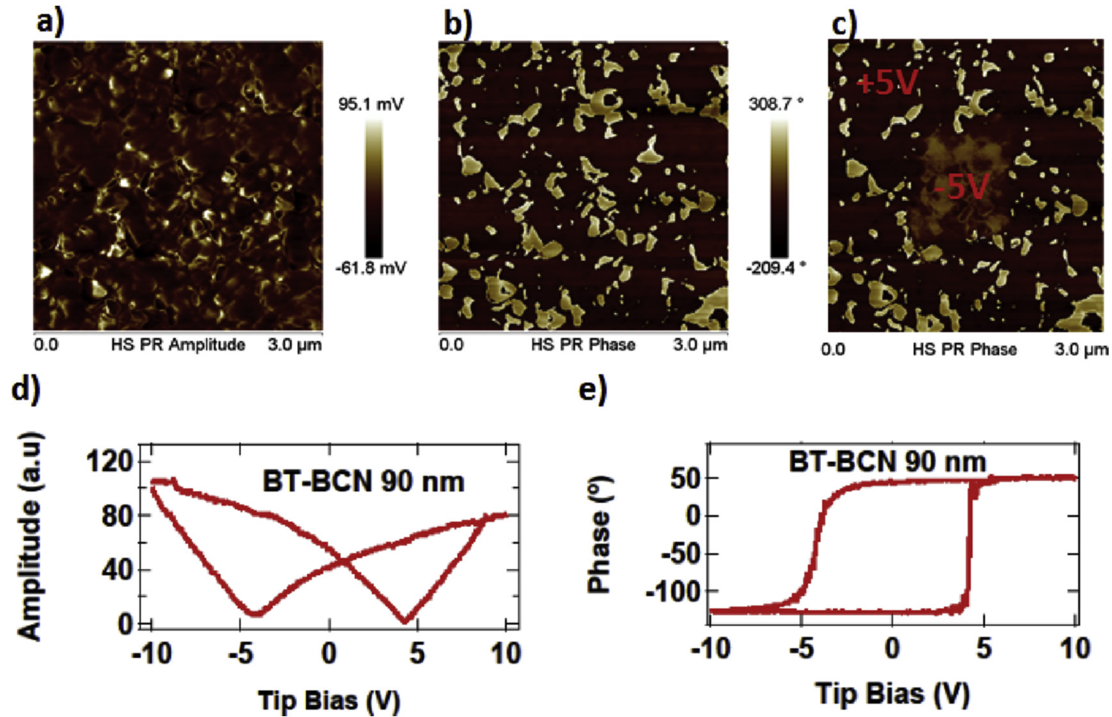

Fig. 2. a) PFM amplitude micrograph of the 90 nm thick BT-BCN film. The phase micrographs can be seen in b), and c), where the phase of the central region was reversed. FE behavior can be shown by the hysteresis in the amplitude and phase component of the PFM, as seen in figures d) and e).

switching behavior in BT-BCN may play a controlling role in determining the field-dependent change of the refractive index [16].

3.2. Variation in the dielectric permittivity

In order to better understand the dielectric behavior of BT- BCN films, the dielectric constant as a function of frequency was measured, as shown in Fig. 3a, for the 120 nm thick sample. For these measurements, Pt electrodes (diameter ~ 200 µm) were deposited on the top surface of the film. One can clearly observe enhanced frequency dispersion of the relative permittivity demonstrating the polar nature of the specimen. We also measured capacitance versus voltage at 200 kHz while sweeping voltage from negative to positive (up) and from positive to negative (down), presented in Fig. 3b. The relative permittivity was found to change significantly with varying bias (V) and exhibited a tunability of 82%. The difference in the peak position during up and down sweeps is due to the presence of the spontaneous polarization. The variation in the dielectric permittivity under applied bias is related to the polarization modulation, which affects the refractive index of the system.

3.3. Reflectometry measurements

Reflectometry measurements were performed in order to measure the index of refraction of BT-BCN. Fig. 4 shows the schematic of the experimental set up. The polarization of the laser, represented in black, is initially s-polarized, and a Glan Cube is employed in order to change the polarization angle. The light then reflects off the sample, which changes the polarization angle due to the differences in the reflection coefficient between s and p-polarized electric field components. The reflected light passes through an analyzer, before reaching to the detector. In our set up, the light source was a 798 nm Ti:sapphire oscillator, with a pulse duration of 100 fs, a repetition rate of 80 MHz, and intensities of up to 3 μW on the sample. An optical chopper with a 331 Hz frequency was employed in order to utilize standard lock-in measurements. The polarization of the reflected light was calculated by varying the analyzer angle, which modulates the intensity as following:

$$I = A cos(\psi - \theta')^2 + B \quad (1a)$$

$$I = (A + c\psi) cos(\psi - \theta')^2 + B \quad (1b)$$

where we define I as the intensity, A represents the amplitude, B is the background level, ψ and θ' are the analyzer and the reflected polarization angles, respectively. Eq. (1a) is for a perfect analyzer, however, if the light passes through the analyzer off center, then the intensity may be modulated due to imperfections in the analyzer. To correct for this, a first order term was added into the equation. This fact is shown in Eq. (1b), where c represents the first order correction. An example of a fit for finding the reflected polarization angle can be seen in Fig. 5a).

Since the polarization angle can be written as:

$$cot(\theta') = \frac{E_s'}{E_p'} = \frac{r_s E_s}{r_p E_p} = q cot(\theta) \quad (2)$$

where θ' (θ) is the polarization direction of the reflected (incident) light, r_s (r_p) is the reflection coefficient for s (p) polarized light, and q being the ratio of the reflection coefficients. The ratio of the reflection coefficients was extracted by fitting cot (θ') = qcot(θ-m), with m being the shift, as included due to imperfections in the analyzer and slight differences between the zero position of the polarizer and analyzer. An example fit for the ratio of reflection coefficients for GaAs can be seen in Fig. 5b). The index of refraction was extracted by using the Fresnel equation, Eq. (3), where the index of refraction for air was already set to 1, ϕ is the incident

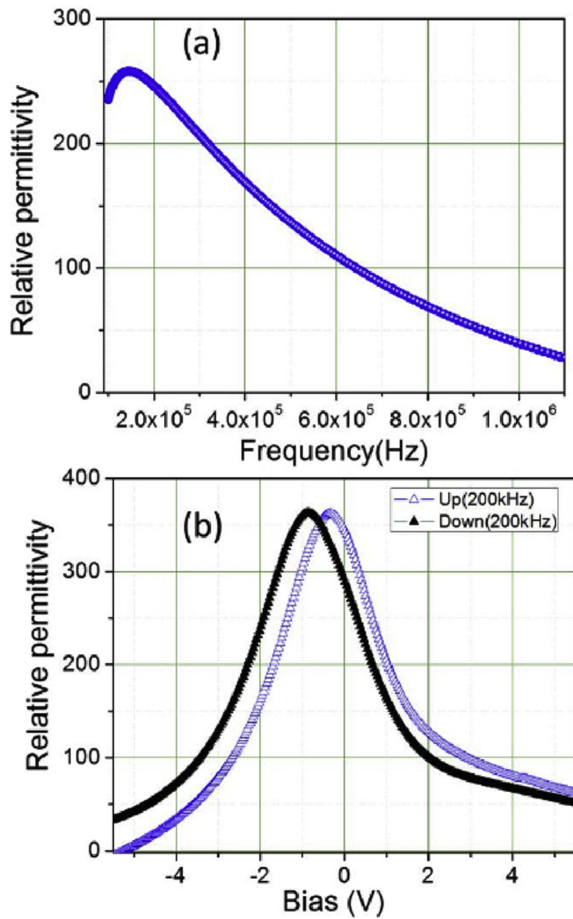

Fig. 3. a) Frequency dependence of relative permittivity. b) Relative permittivity versus bias (V) at 200 kHz.

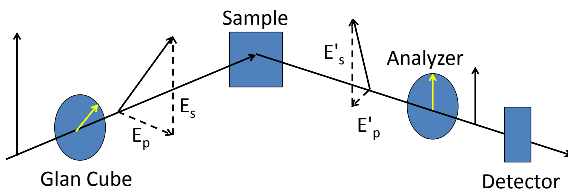

Fig. 4. A schematic of a reflectometry set up. The s-polarized light is passed through a Glan Cube, resulting in the transmitted light being at the angle of the Glan Cube. When the light reflects off the sample, the p-component of the wave changes by 180°, and the polarization direction changes due to the differences in the reflection coefficients for s and p-polarized light. The analyzer modulates the intensity reaching to the detector.

angle, and n is the index of refraction. While BTO is known to exhibit birefringence, the observed birefringence for single domain BTO is within our error bars [17,18].

$$q = \frac{r_s}{r_p} \tag{3}$$

$$r_s = \frac{cos(\phi) - \sqrt{n^2 - sin(\phi)^2}}{cos(\phi) + \sqrt{n^2 - sin(\phi)^2}}$$

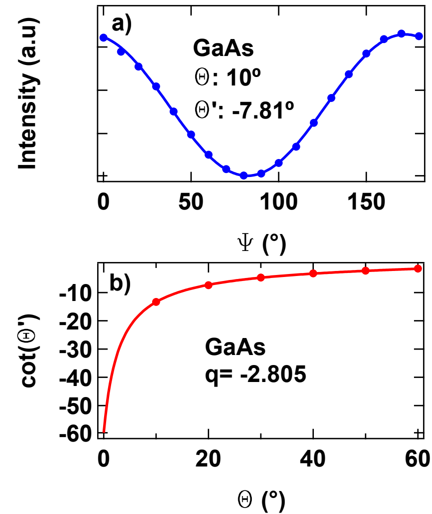

Fig. 5. a Light initially polarized at 10° was reflected off the sample, changing the polarization to −7.81°. The fitting for the reflected polarization was repeated several times for different incident polarizations. Fitting $cot(\theta)$ to the function: q$cot(\theta\text{-}m)$, as seen in b, yields the ratio of the reflection coefficients to be −2.805. Utilizing the Fresnel equation with this value for q yields an incident angle of 62.4°.

$$r_p = \frac{n^2 cos(\phi) - \sqrt{n^2 - sin(\phi)^2}}{n^2 cos(\phi) + \sqrt{n^2 - sin(\phi)^2}}$$

In order to determine the incident angle, first the ratio of the reflection coefficients for GaAs was determined. In this process, using Eq. (3), we were able to calculate the angle of incidence, considering the index of refraction of GaAs to be given by Ref. [19]. After the incident angle was extracted from the GaAs measurements, the refractive index of the BT-BCN sample was measured at least one time, and then the incident angle was determined again by measuring the GaAs sample. If the refractive index for BT-BCN was determined multiple times from a single measurement of GaAs incident angle, the values would be averaged, $\overline{n}(\phi_i)$. The index of refraction shown in Table 1, is given by Eq. (4.1), where the average value of the refractive index per determined incident angle, is averaged over all determined incident angles. The error was calculated as the standard error, given in Eq. (4.1), where the incident angle was determined by repeating the measurements up to 22 times per sample. An example fit for the 120 nm BT-BCN sample can be seen in Fig. 6, whereas examples for the 90 nm and 1.5 nm samples are shown in Figs. 7 and 8, respectively.

$$n = \frac{\sum_i \overline{n}(\phi_i)}{i} \tag{4.1}$$

$$\delta n = \sqrt{\frac{\sum_i (n - \overline{n}(\phi_i))^2}{i*(i-1)}} \tag{4.2}$$

4. Discussion

As summarized in Table 1, the refractive index of the 1.5 nm sample is significantly larger than that of the other two samples, this could be related to the fact that light also can be reflected off of the HfO_2 layer, which would contribute to the change in the polarization direction. With respect to the other two BTBCN samples, the 120 nm thick sample has a higher refractive index than that of

Table 1
A list of refractive indices of BT-BCN from our study and BTO from other published works, along with their crystal structure and growth temperatures. For our work, the reported index of refraction is an average value of several measurements, and the reported error is the standard error of the mean. For other works, we list the refractive indices from a published figure or based off of their fits to the Sellmeier equations.

Sample Thickness (nm)	Index of Refraction	Growth/Anneal T (°C)	Structure	Reference
1.5	2.98 ± 0.03	750	poly x	This Work
90	1.99 ± 0.05	750	poly x	This Work
120	2.53 ± 0.08	800	poly x	This Work
≥1 μm	1.98	27	amorphus	[21]
≥ 1 μm	1.95	227	amorphus	[21]
≥ 1 μm	2.02	327	poly x	[21]
500 nm	2.03	700	poly x	[22,23]
1.3 μm	1.8	300	amorphus	[20]
1.0 μm	1.9	650	poly x	[20]
1.0 μm	2.4	750	poly x	[20]
1.5 μm	2.37		x-stal	[18]

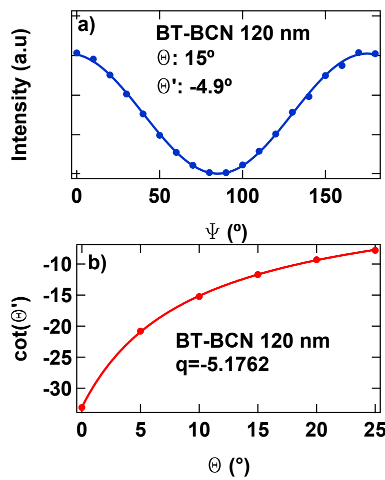

Fig. 6. a) An example of fitting for the reflected polarization with an incident polarization of 15°, for the BT-BCN film with a 120 nm thickness. b) Shows a fit for the ratio of reflection coefficients, q. In this case, q = −5.18, and the angle of incidence was determined from a measurement on GaAs and found to be 61.0°. Thus the calculated index of refraction is 2.5.

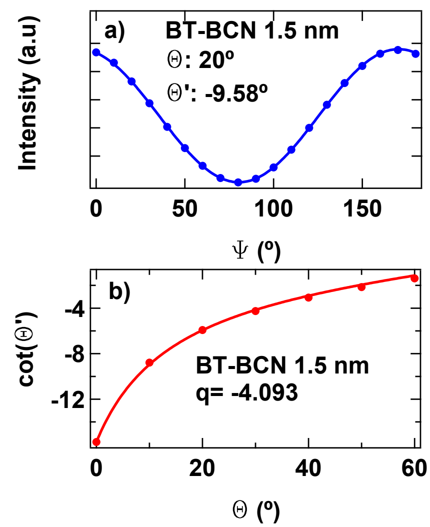

Fig. 8. a) An example of the fitting for the reflected polarization with an incident polarization of 20° for the 1.5 nm thick sample. b) With a ratio of reflection coefficients q = −4.093, and an incident angle of 62.9°, the refractive index was determined to be ≈ 3.0, which is higher than the other two samples.

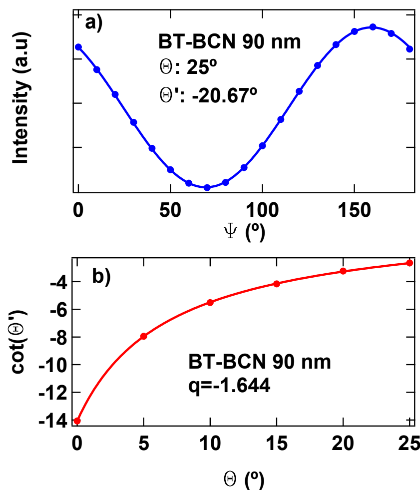

Fig. 7. a) An example showing the fit for the reflected polarization with an incident polarization of 25°, for 90 nm thick BT-BCN. The incident polarization was varied and q was determined by Eq. (2). Panel b) shows the dependence of the incident polarization on the cot(θ'), allowing for the determination of q = −1.64. The angle of incidence was determined to be 37°; which corresponds to a refractive index of 1.97.

the 90 nm thick layer, which was grown at a lower temperature. This behavior is also seen in polycrystalline BTO, as summarized in Table 1, where the refractive indices were taken from their graphs or using their fits to the Sellmeier equation at 798 nm. In Ref. [20], the index of refraction was found to greatly increase with increasing growth temperatures from 600 to 700 °C, which was attributed to crystallization and the formation of larger grain sizes. This could play a part in the increased refractive index of the sample grown at the 800 °C, compared to one at 750 °C, where the growth temperature can result in differences in the domain states. BT-BCN is a tetragonal system having two crystallographically allowed domain variants of 90° and 180°. For example, applying an electric field along an arbitrary direction to a set of two 180° domains, may also result in the rotation of the optical axis within each domain with opposite sign. For both the domains, the phase shift between the ordinary and extraordinary light component will be opposite in the transmitted, elliptically polarized light. The interference of these two polarization states will result in zero net polarization of the transmitted light [14]. Applied fields, higher than the coercive field, switches two 180° domain states to a single 180° domain. On the other hand, 90° domains (with differences in polarization and crystallographic distortions) are difficult to switch. In this case,

despite the two polarization states interfering destructively, they would not cancel out [14]. Therefore, domain structure plays a major role in the EO behavior of a system. The index of refraction obtained for the 1.5 nm thick BT-BCN sample is likely due to a mixture effects from the BT-BCN layer and the HfO_2 layer. The refractive index for the 90 nm film is similar to that of BTO polycrystalline films with a lower growth temperature, whereas the 120 nm thick film has a refractive index closer to that of BTO with a similar growth temperature. In these high quality films, the relative permittivity showed significant variation with the bias voltage which is related to the polarization modulation. Our observations are promising results indicating that improved ferroelectric properties are obtained without compromising the optical properties compared to materials systems such as barium titanate.

Acknowledgment

This material is based upon work supported by the Air Force Office of Scientific Research under award numbers:FA9550-14-1-0376 and FA9550-16-1-0358 under DURIP2016 Program. S.K. and S.G. acknowledge the support from Office of Basic Energy Science, Department of Energy through grant DE-FG02-06ER46290. M.C. acknowledges support from the National Science Foundation through grant ECCS-1507950.

References

[1] A. Chanthbouala, A. Crassous, V. Garcia, K. Bouzehouane, S. Fusil, X. Moya, J. Allibe, B. Dlubak, J. Grollier, S. Xavier, C. Deranlot, A. Moshar, R. Proksch, N. Mathur, M. Bibes, A. Barthélémy, Nat. Nanotechnol. 7 (2012) 101.
[2] R. Guo, L. You, Y. Zhou, Z.S. Lim, X. Zou, L. Chen, R. Ramesh, J. Wang, Nat. Commun. 4 (2013) 1990.
[3] B.A. Magill, K-D Park, Y. Zhou, A. Chopra, Maurya, S. Priya, M.B. Raschke, A. Belyanin, C.J. Stanton, G.A. Khodaparast, Energy Harvest. Syst. 3 (3) (2016) 229.
[4] B.A. Magill, M. Bishop, S.A. McGill, Y. Zhou, A. Chopra, H.-C. Song, C.J. Stanton, S. Priya, G.A. Khodaparast, Proc. of SPIE 9551 (2015), 95510T.
[5] S. Davis, A. Baruth, S. Adenwalla, Appl. Phys. Lett. 97 (2010), 232507.
[6] P. Chen, Gnaydin-Sen, W.J. Ren, Z. Qin, T.V. Brinzari, S. McGill, S.-W. Cheong, J.L. Musfeldt, Phys. Rev. B 86 (2012), 014407.
[7] V. Kalinin, A.A. Demkov, V. Narayanan, Nat. Nanotechnol. 8 (2013) 748754.
[8] D. Maurya, A. Kumar, V. Petkov, J.E. Mahaney, R.S. Katiyar, S. Priya, RSC Adv. 4 (2014) 1283.
[9] D. Maurya, N. Wongdamnern, R. Yimnirun, S. Priya, J. Appl. Phys. 180 (2010), 124111.
[10] D. Maurya, Y. Zhou, B. Chen, M.-G. Kang, P. Nguyen, M.K. Hudait, S. Priya, ACS Appl. Mater. Interfaces 7 (40) (2015) 22458.
[11] S. Kundu, D. Maurya, M. Clavel, Y. Zhou, N.N. Halder, M.K. Hudait, P. Banerji, S. Priya, Sci. Rep. 5 (2015) 8494.
[12] S. Abel, T. Stöferle, C. Marchiori, C. Rossel, M.D. Rossel, R. Erni, D. Caimi, M. Sousa, A. Chelnokov, B.J. Offrein, J. Fompeyrine, Nat. Commun. 4 (2013) 1671.
[13] S. Abel, D. Caimi, M. Sousa, T. Stöferle, C. Rossel, C. Marchiori, A. Chelnokov, J. Fompeyrine, Proc. SPIE 8263 (2012), 82630Y-1.
[14] Vijay Narayanan, Martin M Frank, Alexander A. Demkov (Eds.), Thin Films on Silicon: Electronic and Photonic Applications, World Scientific, 2016.
[15] W.J. Hu, D.M. Juo, L. You, J. Wang, Y.C. Chen, Y.H. Chu, T. Wu, Sci. Rep. 4 (2014) 4772.
[16] M.J. Dicken, L.A. Sweatlock, D. Pacifici, H.J. Lezec, K. Bhattacharya, H.A. Atwater, Nano Lett. 8 (2008) 4048.
[17] K. Buse, S. Riehmann, S. Loheide, H. Hesse, F. Mersch, E. Krätzig, Phys. Stat. Sol. (A) 135 (1993). K87.
[18] A.R. Johnston, J. Appl. Phys. 42 (1971) 3501.
[19] G.E. Jellison Jr., Opt. Mat. 1 (1992) 151.
[20] R. Thomas, D.C. Dube, M.N. Kamalasanan, S. Chandra, Thin Solid Films 346 (1999) 212.
[21] M. Wöhlecke, V. Marrello, A. Onton, J. Appl. Phys. 48 (1997) 1748.
[22] P.C. Joshi, S.B. Desu, Thin Solid Films 300 (1997) 289.
[23] P. Li, J.F. McDonald, T.-M. Lu, J. Appl. Phys. 71 (1992) 5596.

View publication stats